Measurement of Rotor Clearance Using a Dual-electrode Electrostatic Sensor

Xuanda Liu, Yong Yan, *Fellow, IEEE*, Yonghui Hu, *Senior Member, IEEE*, and Lijuan Wang, *Senior Member, IEEE*

***Abstract*—Clearance monitoring of rotors is of importance for the safe operation of mechanical systems. It is essential for the system stability and early warning of faults to monitor the clearance of a rotor. A novel technique is proposed in this paper for the noncontact measurement of the clearance of a metallic rotor through electret-assisted electrostatic sensing and correlation signal processing. A single charged electret marker is used as a tracer and attached to the surface of the rotor as a stable charge source for the electrostatic sensors. The clearance measurement is inferred from the rotational speed measured through autocorrelation and the transit time measured through cross-correlation. A geometric relationship between the electrode position and the rotor axis is established. A series of experimental tests were conducted in a temperature and humidity-controlled chamber to evaluate the impact of ambient conditions on the performance of the sensor. Experimental results suggest that, an increase in ambient temperature and relative humidity has a minimal impact on the correlation characteristics of signals. Within the speed range of 120 – 3000 rpm, this technique enables the measurement of the metallic rotor clearance across the range of 2 – 18 mm, with a relative error within ±6%.**

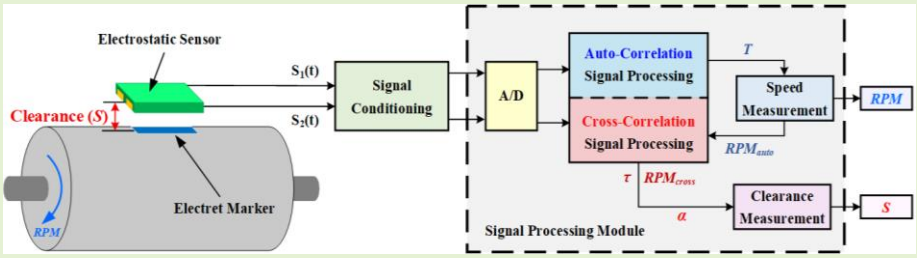

***Index Terms*—Clearance measurement, electrostatic sensors, electret marker, metallic rotor, rotational speed.**

I. Introduction

ROTATING machinery is widely utilized across various industrial sectors, such as turbines, engines, and generators. Rotational speed is one of the crucial indicators reflecting the operational status of a rotor. Additionally, continuous operation of the rotor over a long period of time may cause mechanical wear and vibration, which in turn may result in changes in the clearance of the stationary part with reference to the rotor, posing a potential risk of collisions between the rotor and other components [1]. Therefore, the accurate determination of the clearance between the rotor and other stationary components in a mechanical system is essential for maintaining operation efficiency, reducing wear, preventing catastrophic failures, and improving system reliability, particularly in large-scale systems such as wind turbines and gas turbines [2], [3].

Over the years, several methods have been developed to achieve non-contact clearance or displacement measurement. Well-established techniques such as optical, capacitive, ultrasonic, and magnetic sensors have been employed in different application scenarios [4], [5]. Ren *et al.* [6] used laser sweep frequency interferometry combined with time-frequency domain signal processing algorithms to achieve axial clearance measurement in high-speed rotating machinery. Lavagnoli *et al.* [7] described a capacitance-based clearance measurement technique through detecting changes in capacitance between static and rotating components. Josef *et al.* [8] investigated a digital eddy current position sensor based on the oscillator injection locking principle. These techniques have high sensitivity and resolution. However, such methods are highly material-dependent and have weaknesses such as complex structure, high cost, complicated calibration, and susceptibility to environmental influences. Furthermore, their sensitivity is often limited when dealing with non-conductive targets.

The utilization of electrostatic sensors has gained considerable attention in recent years due to their non-contact nature, high sensitivity, ease of installation and maintenance, and low cost. However, reported studies on using electrostatic sensors for clearance or displacement measurement are quite limited. Electrostatic sensors, in conjunction with signal

Manuscript received xx, xx; revised xx xx, xx; accepted September xx, xx. Date of publication October xx, xx; date of current version November xx, xx. This work was supported by the National Natural Science Foundation of China under Grant 51375163. The associate editor coordinating the review of this article and approving it for publication was xx. *(Corresponding author: Yong Yan.)*

Xuanda Liu and Yonghui Hu are with the School of Control and Computer Engineering, North China Electric Power University, Beijing 102206, China (e-mail: Liuxd@ncepu.edu.cn; huyhui@gmail.com).

Yong Yan is with Hangzhou International Innovation Institute, Beihang University, Hangzhou 311115, China (e-mail: yongyan@buaa.edu.cn).

Lijuan Wang is with the School of Engineering, University of Kent, Canterbury, Kent CT2 7NT, UK (e-mail: l.wang@kent.ac.uk).

This article has been accepted for publication in IEEE Sensors Journal. This is the author's version which has not been fully edited and
content may change prior to final publication. Citation information: DOI 10.1109/JSEN.2025.3528445

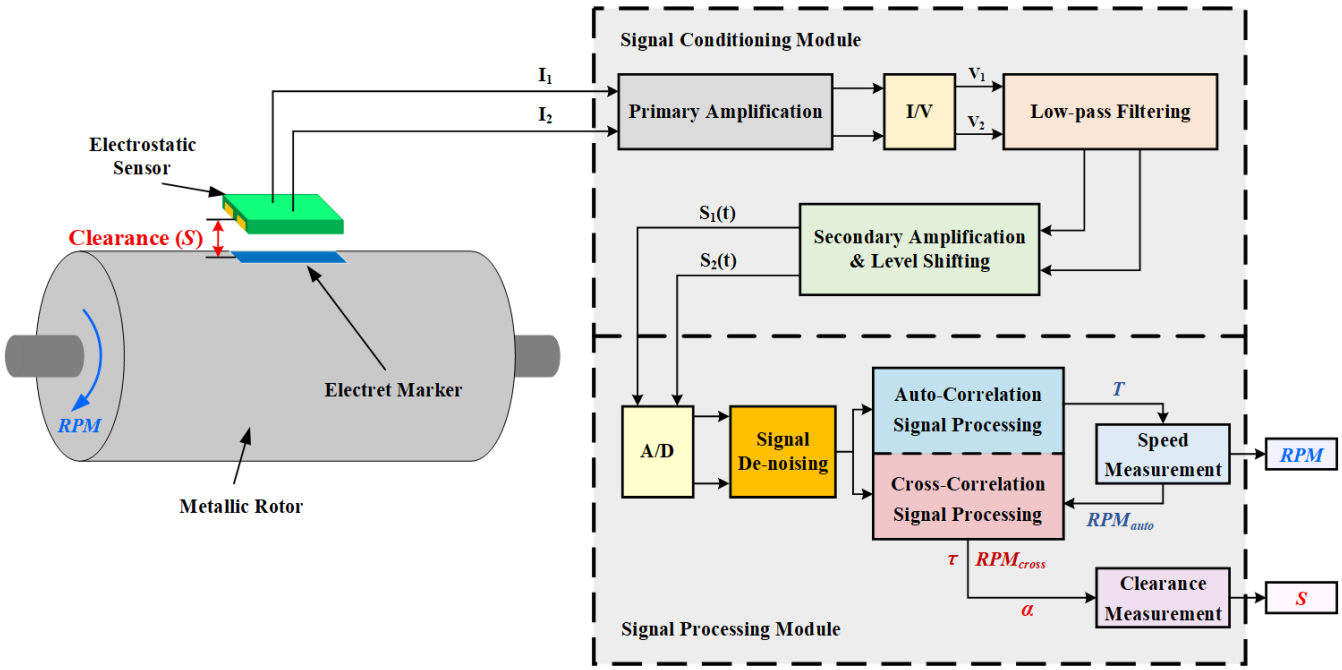

Fig. 1. Principle of the clearance measurement system.

processing methods such as correlation analysis, mode decomposition, and time-frequency-domain analysis, have been utilized for vibration detection of rotational and translational mechanical components in steady motion [9], [10]. Wang *et al.* [11] proposed a method for recognizing the radial vibration in non-metallic rotors by applying multiple electrostatic sensors combined with the Hilbert-Huang transform. Owing to the charge quantity on the rotor surface being uncertain, the method can only be used to measure the vibration frequency but not the absolute displacement of the rotor. Moreover, the installation of multiple sensors requires a complicated mechanical structure. To overcome the dependency of electrostatic sensors on the material of the target and improve both the signal quality and rangeability, electret markers are used instead of traditional dielectric on the rotor surface [12], [13]. Nevertheless, variations in ambient conditions (temperature and relative humidity) may cause significant fluctuations in the charge level on the electrodes, which in turn affect the strength of the sensor signals. This impact on electrostatic sensor performance for displacement measurement cannot be ignored and requires quantitative analysis [14], [15]. The frequency domain method is also used to measure the vibration of an imbalanced rotor [12], but this approach requires pre-calibration of the sensor, and the impact of model accuracy on the measurement results remains to be examined.

In summary, installation complexity, material dependence, and absolute displacement measurement are key challenges that need to be addressed when implementing electrostatic sensors for clearance or displacement measurement.

The innovation of this paper lies in proposing a new technique for the measurement of the clearance between the rotor and the stationary component that does not depend on signal strength. Unlike traditional displacement sensors (such as eddy-current sensors), it is characterized by a simple design, independence from specific target materials, no need for complex calibration, and strong adaptability to different environmental conditions. In this paper, a dual-electrode electrostatic sensor is used for monitoring the clearance of a metallic rotor - the term "clearance" is defined as the vertical distance between the stationary sensor board the rotating surface. With the aid of correlation signal processing algorithms, a geometric relationship between the electrode position and the rotor axis is established, thereby enabling the measurement of the rotor axial position and clearance by integrating the measured rotational speed with geometric relationships. Through a series of experimentations, the performance of the sensor for clearance measurement of the rotor is assessed in detail. Moreover, the effect of ambient conditions on the output response of the sensor for clearance measurement of the rotor is quantified.

II. Methodology

A. Measurement Principle and Method

The overall principle of the clearance measurement system is shown in Fig. 1, which consists of the electret marker, electrostatic sensing unit, signal conditioning module, and signal processing module.

The operation of the electrostatic sensor relies on the electrostatic induction effect between the triboelectric charge and induced charge. Due to the conductivity of the metallic rotor, triboelectric charge cannot be generated and retained on its surface during rotation. Unlike the rotor made of non-metallic materials, electrostatic induction does not occur between the electrodes and the surface of the metallic rotor and hence no effective signals from the electrostatic sensor. To address this problem, an electret film marker carrying a certain quantity of charge is affixed to the metallic rotor surface as a tracer to reflect the motion trajectory of the metallic rotor. Because of the capacity of the fluorinated ethylene propylene (FEP) electret material to retain charge for a long time and the high stability of negative charge storage [16], [17], the FEP electret marker is negatively charged by a high-voltage needle

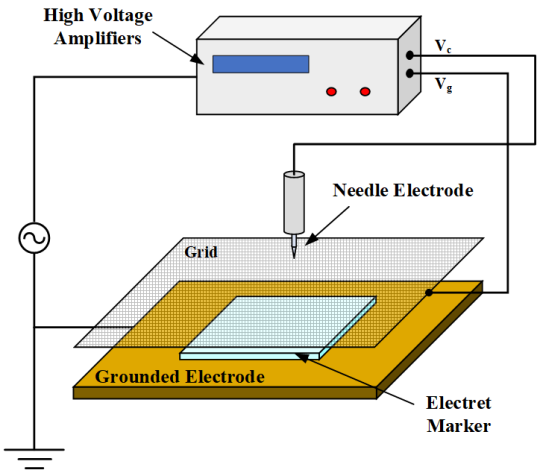

Fig. 2. Schematic of the charge process for electret markers.

source (Fig. 2). Then the injected charge deposits on the surface of the electret material and remains there for a long period. During the rotation, friction with air contributes to additional charge accumulation on the surface. The marker provides the required stable source charge on the rotor for electrostatic induction, which is contributed to improve the sensitivity and rangeability of electrostatic sensors.

During the rotation process, the electret marker is further charged due to the triboelectric charging effect. A dual-electrode electrostatic sensor is installed near the metallic rotor and used to sense the fluctuation of surface charge on the marker. Subsequently, the variation in charge is output in the form of current and enters the signal conditioning module. The current is converted into a voltage signal, followed by low-pass filtering and secondary amplification. Finally, signals are collected and processed in the signal processing module to determine the rotor clearance (S) (Fig. 1).

The upstream signal $S_1(t)$ and downstream signal $S_2(t)$ from the sensor are both periodical with a period (T) representing the time taken for the rotor to make a complete revolution. The period is determined from the autocorrelation functions of the signal. Time difference between output signals from two electrodes corresponds to the transit time (τ), i.e. the time it takes for the electret marker to rotate through the two electrodes. The transit time is obtained from the cross-correlation function of the two signals [9]. A typical example of the sensor signal waveforms and resulting correlation functions is shown in Fig. 3. The locations of the dominant peaks in the correlation functions are used to determine T and τ, respectively. Subsequently, the rotational speeds derived using the two correlation algorithms are represented as

$$\begin{cases} RPM_{auto} = \dfrac{60}{T} \\ RPM_{cross} = \dfrac{30\alpha}{\pi\tau} \end{cases} \tag{1}$$

where α denotes the angle between the centers of the two electrodes relative to the rotational axis of the rotor (Fig. 1). Theoretically, the rotational speed measurement results yielded

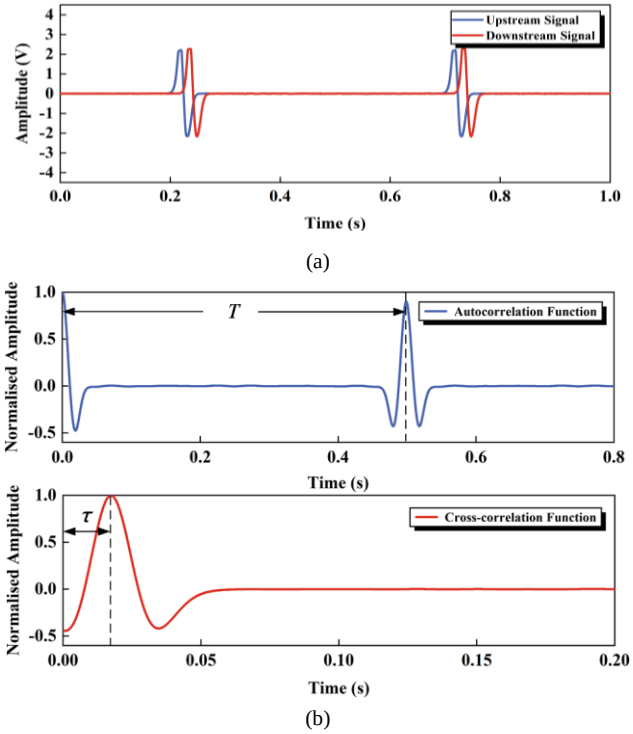

Fig. 3. Typical example of the sensor signal waveforms and resulting correlation functions. (a) Output signals. (b) Autocorrelation and cross-correlation functions.

by autocorrelation and cross-correlation are both equal and accurate. However, in the practical measurement cycle, the sampling frequency (f_s) has a significant impact on the accuracy of the correlation signal processing algorithms. The sampling data length (l_s) influences the minimum measurable speed of autocorrelation and cross-correlation algorithms [18]. For the proposed system in this paper, when the f_s and l_s are set as constant, the cross-correlation algorithm is capable of achieving lower rotational speed measurements compared to the autocorrelation algorithm. The lower speed limit ($RPM_{auto\min}$) of the autocorrelation algorithm is regarded as the switching threshold (RPM_{th}) between the two algorithms [18], i.e.,

$$RPM_{th} = RPM_{auto\min} = \frac{120}{l_s} \tag{2}$$

When the rotational speed exceeds the threshold, the system is able to acquire both autocorrelation and cross-correlation speeds. The proposed technique for clearance measurement of the rotor is also based on the principle of correlation signal processing. In practical experiments, the accuracy of the two algorithms is significantly influenced by the sampling frequency of the measurement system and the installation conditions of the electrostatic sensor. Previous research has demonstrated that autocorrelation algorithms have higher accuracy in speed measurement than the cross-correlation algorithm [18]. As shown in (1), it is clear that the measurement error in autocorrelation speed arises solely from the error in determining the period (T), whereas the accuracy of cross-correlation speed depends on central angle (α) and transit time (τ). At a given sampling frequency and rotational speed, the

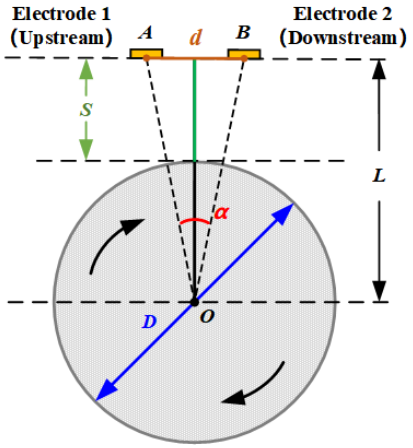

Fig. 4. Geometric schematic of the rotor and the sensor board.

period (T) is much greater than the transit time (τ), resulting in a higher number of sampling points within the data length (l_s) and thus achieving higher accuracy.

The spatial geometric location of the rotor and the dual-electrode sensor board is shown in Fig. 4, assuming that the centers of the two electrodes are located at A and B, respectively, with a spacing of d, and the diameter of the rotor is D.

For traditional cross-correlation measurement, as shown in (3), α is calculated based on the manually measured distance from the sensor to the rotor surface (S), which inevitably introduces the measurement error.

$$\alpha = 2\tan^{-1}\frac{d}{2\left(\frac{D}{2}+S\right)} \tag{3}$$

On the contrary, if incorporating the speed via autocorrelation into the cross-correlation algorithm, α can be derived more accurately from

$$\alpha = RPM_{auto}\cdot\frac{\pi\tau}{30} = \frac{2\pi\tau}{T} \tag{4}$$

Then, the distance from the rotor axis to the sensor board L, and the clearance between the rotor surface and the sensor S, are determined respectively, from

$$L = \frac{d}{2\tan\frac{\alpha}{2}} = \frac{d}{2\tan\frac{\pi\tau}{T}} \tag{5}$$

$$S = L - \frac{D}{2} = \frac{d}{2\tan\frac{\pi\tau}{T}} - \frac{D}{2} \tag{6}$$

In this way, the measurement of the rotor clearance is achieved at the same time as the rotational speed measurement.

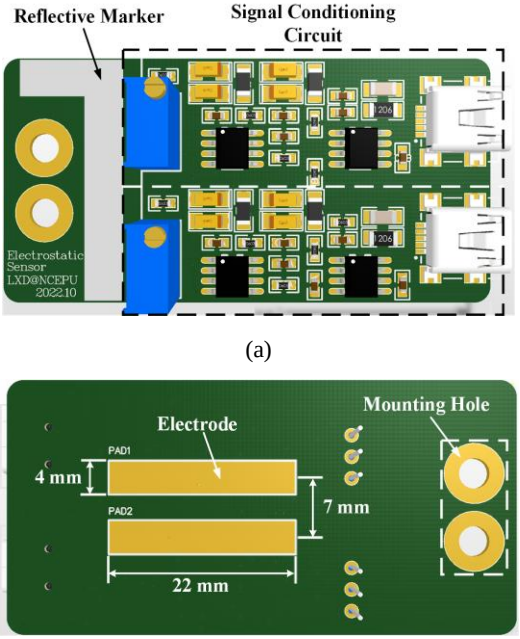

Fig. 5. Structure of the sensor board and electret marker. (a) Top view of electrostatic sensor. (b) Bottom view of electrostatic sensor. (c) Electret marker and PCB.

B. Sensor and Marker Design

In earlier research [18], the finite element modeling of the dual-electrode electrostatic sensor, as well as the parameter optimisation of the electrodes and markers, have been systematically introduced. In this paper, the size of the electrodes and the marker are designed to fall within the optimal range given by [18]. The diameter (D) of the tested rotor in this work is 60 mm. Two strip-shaped electrodes and a signal conditioning circuit are integrated into a small printed circuit board (PCB) (Fig. 5(a)). A second-order Sallen-Key low-pass filter with a cut-off frequency of 1.59 kHz is employed to remove high-frequency noise and provide antialiasing in the A/D conversion. To minimize the effect of time delay of the signals through the filters on cross-correlation results, the

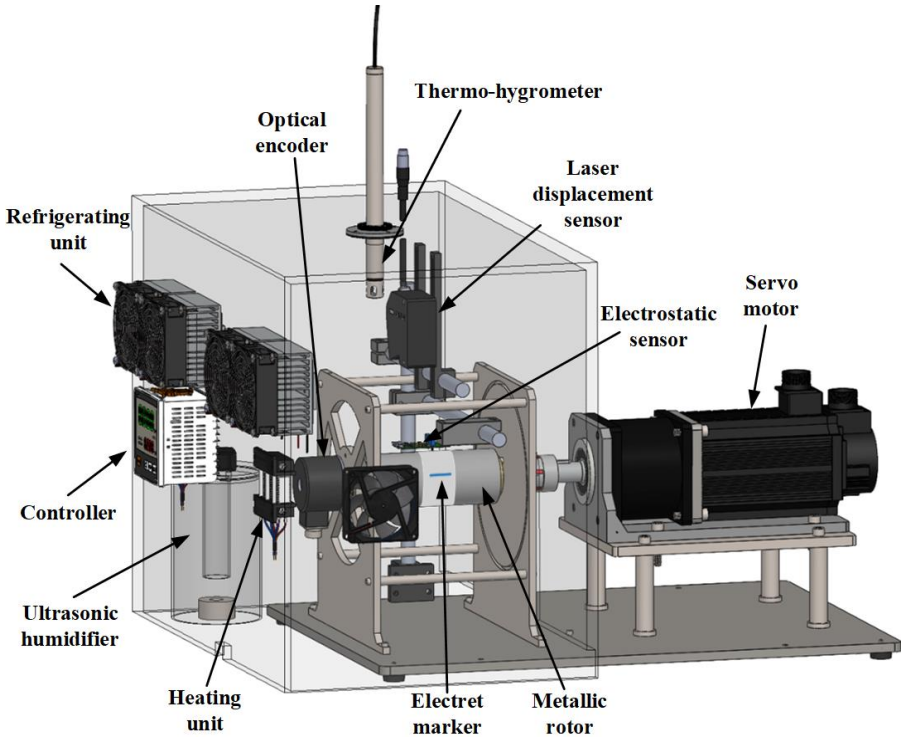

Fig. 6. Test rig.

components in the filters are trimmed to be identical. To facilitate the calibration of the height of the sensor board and obtain the reference value of the sensor-rotor distance, an area is reserved on the front of the sensor board for attaching the reflection marker required by the reference laser clearance sensor. The layout of the two electrodes is shown in Fig. 5 (b), the electrode length is 22 mm, and the width is 4 mm. There is a spacing of 7 mm between the centers of the two electrodes. Due to the best testing performance, the strip-shaped electret marker is made of fluorinated ethylene propylene (FEP) and is designed as 22 mm × 2 mm (see Fig. 5(c)).

III. Experiments and Results

A. Experimental Setup

An experimental test rig for simultaneous measurement of rotor clearance and rotational speed, was designed and constructed. A metallic rotor with a diameter of 60 mm is connected to a servo motor, with an adjustable speed from 0 to 3000 rpm. The sensor board is mounted on a precision lifting platform for precise height adjustment. The adjustment of the clearance between the rotor and the sensor board is achieved by altering the height of the sensor board. An inclinometer is used to calibrate the attitude deviation between the sensor and the rotor, minimizing the impact of attitude difference on the measurement results. In this study, the sampling frequency of the measurement system is set as f_s = 100 kHz, and the data length for a single correlation analysis is set as l_s = 1 s. In this case, the threshold speed is RPM_{th}=120 rpm. A low-cost FEP marker, with 22 mm in length, 2 mm in width, 150 μm in thickness, and roughness of *Ra*-0.43, is charged for 15 min using a grid-controlled corona discharge device with a voltage of –15 kV. The titanium grid voltage is set to –0.8 kV, and after charging, the potential of the electret surface is approximately equal to the grid potential. The electret marker is then fixed on the surface of the rotor. The reference sensor for rotational speed measurement is a high-precision optical encoder (Atonics, model E40H12). A commercial laser displacement sensor (Keyence, model LK-H085) with an accuracy of ±0.1 μm, is applied to obtain the reference value to assess the effectiveness of the rotor clearance measurement.

To analyse the impact of ambient conditions (temperature and relative humidity) on the operation performance of electrostatic sensors, all the experiments were conducted in a transparent chamber with controllable temperature and relative humidity. The chamber is equipped with a controller, a heating unit, a refrigerating unit, an ultrasonic humidifier, and a thermo-hygrometer for temperature and humidity monitoring (see Fig. 6). The ambient temperature was adjustable between 10°C and 60°C, and the relative humidity ranged from 20% to 90%. Fig. 6 shows the overall assembly diagram of the test rig.

B. Effect of Electret Charging Duration on Electrostatic Sensors

To maximize the sensor sensitivity, the electret marker used as a tracer should carry as much injected charge as possible. The charging duration significantly affects the surface potential and the amount of charge on the electret marker. Therefore, under given ambient conditions, it is essential to determine the optimal charging duration.

Under the ambient conditions of 21°C and 55% relative humidity, FEP markers were charged for different durations and then attached to the rotor surface separately. To quantify the impact of charging duration on the output response of the electrostatic sensor, root mean square (rms) values of the output signals are obtained at the threshold rotational speed (RPM_{th}=120 rpm). To remove high-frequency noise and achieve a smoother output, the signal from the sensor is first

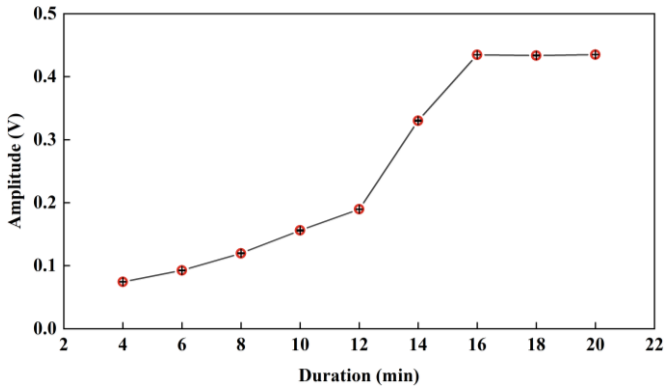

Fig. 7. rms amplitude as a function of charging duration at the speed of 120 rpm.

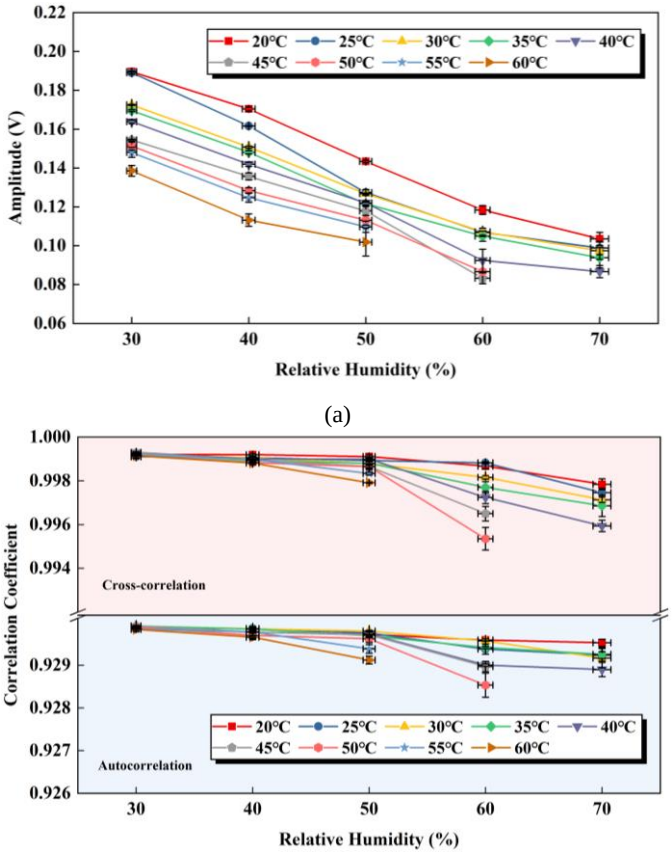

Fig. 8. Signal strength and correlation coefficients as a function of relative humidity for various test temperatures. (a) rms amplitude. (b) Correlation coefficients.

processed through filtering. From Fig. 7, it can be seen that the rms amplitude of the signal increases with the charging duration of the marker, indicating that the amount of injected charge on the marker surface also increases. When the charging duration exceeds 16 min, the amount of injected charge reaches the maximum storage capacity of the FEP electret material. At this point, the injected charge becomes saturated, and the strength of the output response ceases to change significantly. Therefore, for the FEP electret film used in this study, the optimal charging duration is determined to be 16 min.

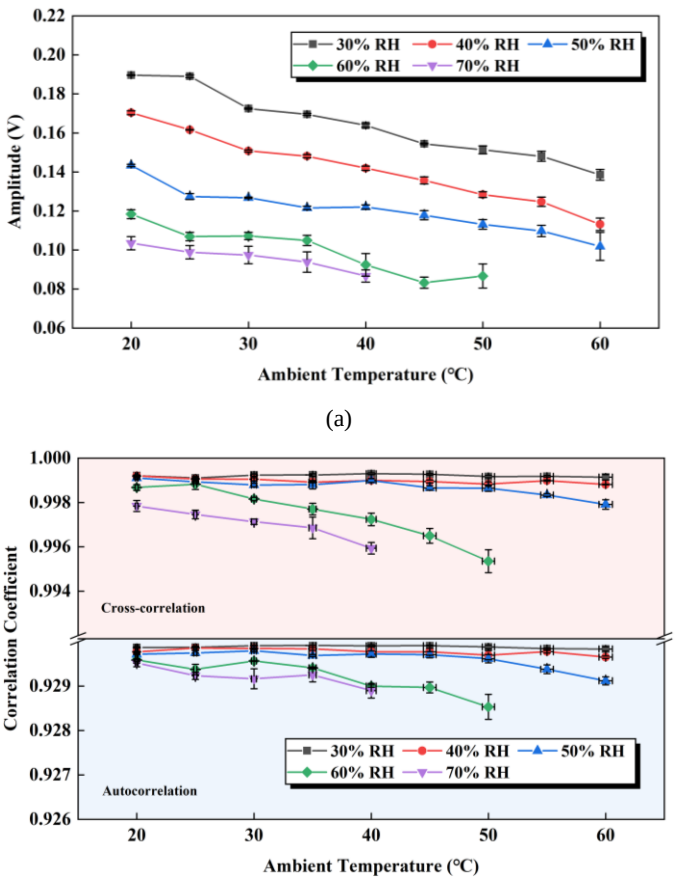

Fig. 9. Signal strength and correlation coefficients as a function of temperature for various relative humidities. (a) rms amplitude. (b) Correlation coefficients.

C. Effect of ambient conditions on electrostatic sensor

Signal quality is one of the key factors affecting the performance of clearance measurement. During the rotation process, due to the triboelectric effect, the charge level on the electret marker surface varies dynamically and unpredictably with the variation in rotational speed. In addition to rotational speed, ambient conditions such as temperature and relative humidity also have significant effects on the triboelectric charging and discharging process, and the charge retention capability of the electret marker. The rms amplitude and correlational coefficient of the output signal are obtained to quantify the impact of ambient factors on the operation performance of the electrostatic sensor. The temperature and humidity of the test environment were adjusted and maintained by a controller. All experiments were conducted at a given rotational speed of 120 rpm. It is worth noting that in practical applications, high temperature and high humidity cannot be achieved simultaneously because, at higher temperatures, moisture quickly condenses on the metallic rotor surface and surrounding components.

Following the control variable method, the ambient temperature is set as a constant, while the relative humidity is varied from 30% to 70%, then the impact of relative humidity on the output response is shown in Fig. 8(a). The results imply

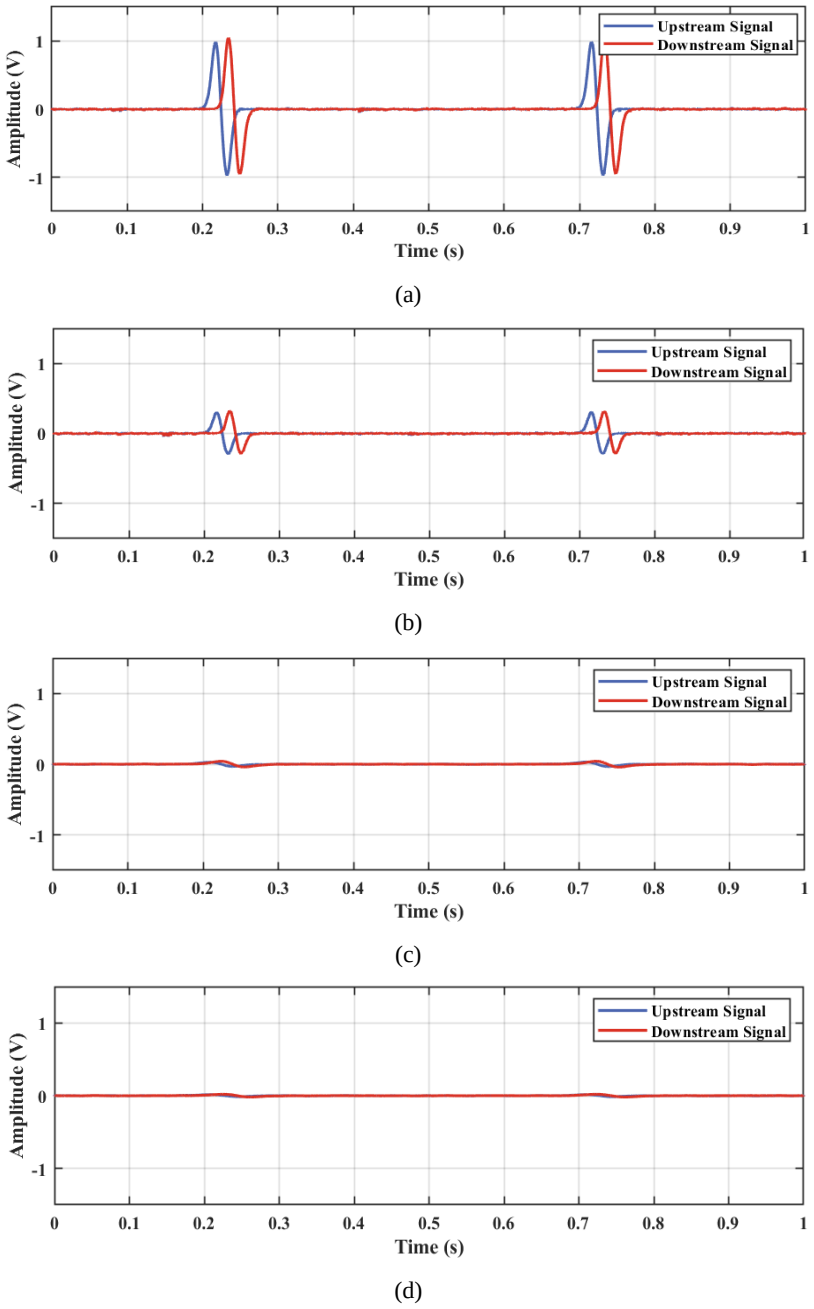

Fig. 10. Output response of the electrostatic sensor for four different rotor clearance cases. (a) 2 mm. (b) 8mm. (c) 14mm. (d) 18mm.

that, at a given temperature, an increase in relative humidity causes a reduction in the signal strength. This is attributed to the fact that higher humidity levels introduce more water molecules into the air, and more conductive pathways accelerate the leakage of electrostatic charge carried by the marker and the electrode. Additionally, with the increase in relative humidity, the electrostatic signals still exhibit a stable similarity, with the correlation coefficients decreasing slightly. The autocorrelation coefficient and cross-correlation coefficient remain above 0.928 and 0.995, respectively (Fig. 8(b)).

Similarly, the ambient relative humidity is set as constant, and the rms amplitude and correlation coefficient of the signal are obtained while varying the temperature from 20°C to 60°C.

Fig. 9(a) illustrates that at a given relative humidity, as the temperature increases, the signal strength decreases, indicating a reduced accumulation of charge on the electrode and marker surface. This can be interpreted as being due to increased mobility of the surface charge caused by an increase in the ambient temperature, leading to a faster dissipation of surface charge. Ambient temperature similarly has a minimal impact on the correlation coefficients of electrostatic signals.

Therefore, ambient conditions (temperature, and relative humidity) significantly affect the output response strength of the electrostatic sensor. In contrast, correlation characteristics are less affected. For this reason, the signal amplitude cannot be used reliably to quantify the variation in rotor clearance.

D. Clearance measurement results

A set of experiments was conducted at rotational speeds above the threshold (120 rpm) to verify the effectiveness of the electrostatic sensor in measuring rotor clearance. Fig. 10 shows

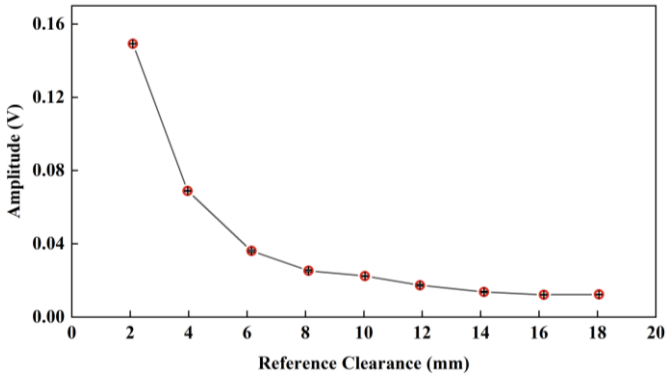

Fig. 11. rms amplitude as a function of rotor clearance.

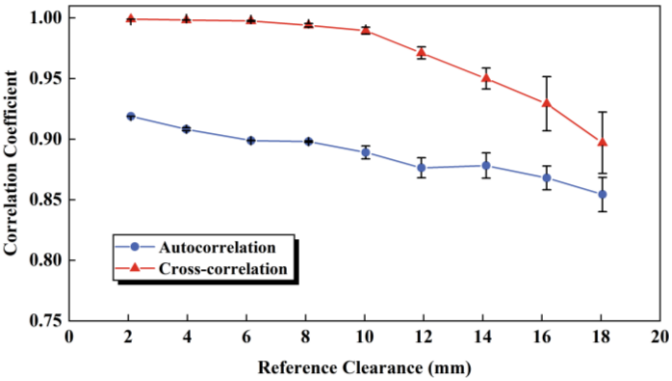

Fig. 12. Correlation coefficients as a function of rotor clearance.

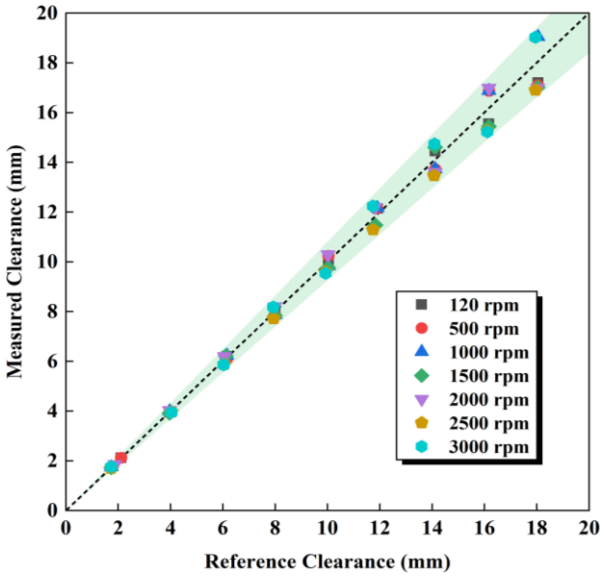

Fig. 13. Comparison of clearance measurement results.

the waveform of typical signals from the electrostatic sensor at a rotational speed of 120 rpm for a rotor clearance of 2, 8, 14, and 18 mm. When the electret marker is used as a tracer attached to the rotor surface, distinct pulse waveforms are observed in both the upstream and downstream output signals from the sensor during rotation. However, when the rotor clearance exceeds 18 mm, the electrostatic induction between the marker and the electrodes becomes very weak, resulting in a poor signal-to-noise ratio in the output response from the sensor. At this point, it is hard to achieve effective rotational

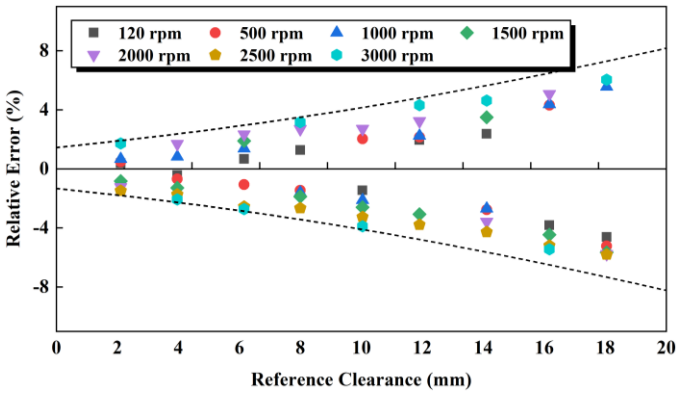

Fig. 14. Relative error of the measured clearance at constant speed.

speed and clearance measurements. Furthermore, manufacturing differences in the processing of electronic components in the signal conditioning circuit result in minor discrepancies in the pulse amplitudes of the output signals.

The rms amplitude for different clearances is presented in Fig. 11. It is obvious that, as the clearance increases, the sensitivity of the electrode to the inducing charge decreases rapidly, hence the strength of the output signal becomes weaker. In cases where the clearance increases beyond 14 mm, due to the weakened pulse response, the proportion of effective pulses in the signal decreases, hence there is no significant decrease observed in the rms amplitude of the signal.

Fig. 12 shows the relationship between the correlation coefficient of the signals and the rotor clearance. It can be observed as the clearance increases, the correlation coefficients decrease but remain at a relatively high level. Specifically, the autocorrelation coefficient consistently stays above 0.85, while the cross-correlation coefficient remains above 0.9 (Fig. 12). This is attributed that, even though an increase in clearance leads to a sharp decline in signal strength, it does not alter the periodicity of the signal itself nor the similarity between signals. It is precisely because of the stable existence of signal correlation features that the correlation signal processing algorithm is an effective method for clearance measurement. Additionally, the reduction in signal quality leads to reduced similarity between the upstream and downstream signals. Therefore, the cross-correlation coefficient exhibits a more significant decline compared to the autocorrelation coefficient.

The periodicity and similarity characteristics (T and τ) of the electrostatic signal at different rotational speeds are described by the correlation functions. Subsequently, the signal period (T) is used to calculate the autocorrelation-based rotational speed, which is then integrated into (4) to derive the angle (α) between the centers of the two electrodes. Finally, the clearance (S) is obtained based on (6).

Fig. 13 presents a comparison of the clearance measurement results with the reference values across the measurement range from 2 to 18 mm, at rotational speeds from 120 to 3000 rpm. Each data point represents the overall average of 20 repeated measurements. The measured values demonstrate a better agreement with the reference values at smaller clearances, while with increasing clearance, slight deviations between the two are observed.

The relative error between the measured and reference clearance is illustrated in Fig. 14. From Fig. 14, it can be

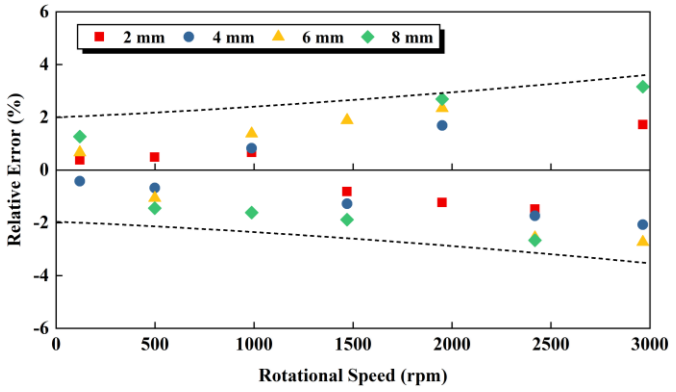

(a)

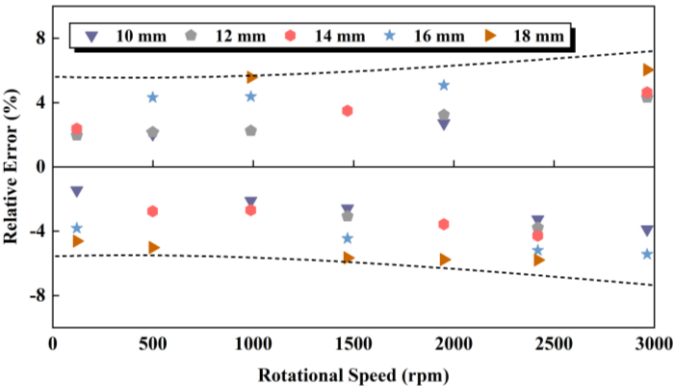

(b)

Fig. 15. Relative error of the measured clearance as a function of rotational speed. (a) 2 – 8mm. (b) 10 – 18mm.

observed that, as the clearance increases at a constant speed, the deviation between the measured and reference values increases gradually. This is attributed to the high sensitivity of the electrostatic induction to changes in sensing distance, where the quality and strength of signals decrease sharply with clearance, resulting in an increase in the relative error of signal period (T) and transit time (τ). Furthermore, at a given rotational speed, an increase in clearance results in a reduction in the central angle (α), leading to a shorter transit time τ. For a given data sampling frequency (f_s), the number of sampling points within the transit time (τ) in cross-correlation algorithm decreases, resulting in an increased relative error. This is another reason for the increase in the measurement error.

Indeed, the accuracy of correlation signal processing algorithms is also related to the rotation speed, which in turn affects the accuracy of clearance measurement. At the constant rotor clearance, the impact of the speed on the accuracy of measured clearance is shown in Fig. 15(a) and (b). As the speed increases, the overall error in clearance measurement also increases due to the fact that the rotational period and the transit time shorten with the increasing speed, which causes an increased error in determining T and τ at a fixed sampling frequency. Therefore, the measurement accuracy of the rotor clearance is higher at lower speeds. The accuracy of the clearance measurement is better than ±6% over the range of 2 18 mm. In summary, the measurement error of rotor clearance primarily depends on the positioning error of the dominant peak during the correlation signal processing. Therefore, it is

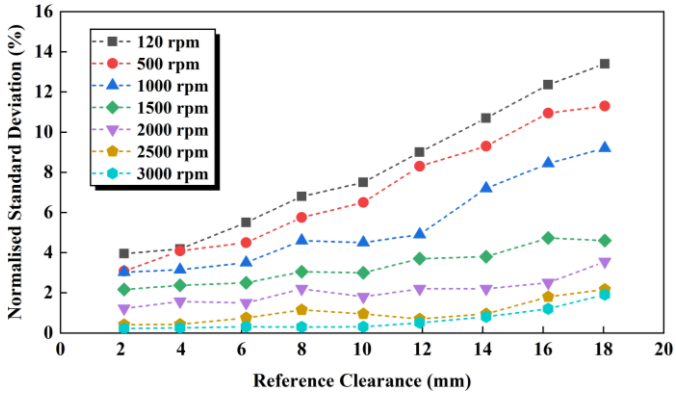

Fig. 16. Normalised standard deviation of the measured clearance.

necessary to optimize the correlation signal processing algorithms in future research to improve measurement accuracy. Moreover, a detailed sensitivity analysis to quantify the effect of attitude differences will be considered in future work.

The clearance measurement repeatability of the proposed system is illustrated in Fig. 16, evaluated by the normalised standard deviation. Fig. 16 shows that the normalised standard deviation between repeated measurement results does not exceed 13% within the clearance range of 2 – 18 mm. Due to the reduction in signal quality when the sensor is further away from the rotor, the repeatability of the system deteriorates with the rotor clearance. When the clearance exceeds 18 mm, due to the extremely low signal quality, the pulse signal is almost buried by noise. At this point, the correlation algorithms are unable to extract valid periodic and similarity features from signals, rendering the clearance measurement results unreliable. The lower limit of clearance measurement depends on the minimum safe distance required for sensor installation. Therefore, the rangeability of the clearance measurement system proposed in this paper is 2 – 18 mm. Additionally, at the given clearance, a higher rotational speed leads to more accumulation of surface charge on the marker, stabilizing the correlation characteristics of signals, and thereby resulting in an improved repeatability of the system.

IV. Conclusions

The measurement of the clearance between the metallic rotor and the sensor board has been implemented using an electrostatic sensor with an electret marker on the rotor. The influence of the charging duration of the electret marker, along with ambient conditions (temperature and relative humidity), on the output signal of the sensing system has been studied. It can be concluded that, for the FEP electret marker used, a charging duration of 16 min is optimal. Increases in ambient temperature and relative humidity degrade signal strength but do not significantly affect the correlation characteristics of the signal. Electrostatic sensors are proven to be adaptable to complex operation environments. The proposed method for rotor clearance measurement has also been validated experimentally. The experimental results have indicated the measurement system enables the measurement of the clearance between the rotor and the sensor, achieving an accuracy of better than ±6% within the rangeability of 2 – 18 mm. Additionally, the clearance measurement is achieved

simultaneously with the concurrent rotational speed measurement. Future research will focus on applying the electrostatic sensing technique to monitor the vibration and clearance of unbalanced rotors.

REFERENCES

[1] V. Patil and P. V. Jadhav, "Dynamic response analysis of unbalanced rotor-bearing system with internal radial clearance," *SN Appl. Sci.*, vol. 2, Oct. 2020, Art. no. 1826.

[2] M. Hossain, A. Abu-Siada, and S. Muyeen, "Methods for advanced wind turbine condition monitoring and early diagnosis: A literature review," *Energies*, vol. 11, no. 5, May 2018, Art. no. 1309.

[3] S. Lee, G. Stone, J. Antonino-Daviu, K. Gyftakis, E. Strangas, P. Maussion, and C. Platero, "Condition monitoring of industrial electric machines: State of the art and future challenges," *IEEE Ind. Electron. M.,* vol. 14, pp. 158-167, Dec. 2020.

[4] A. Ermolaev, B. Gordeev, S. Okhulkov, G. Panovko, and A. Plekhov, "Measuring of rotating shafts angular deformation by means of ultrasonic vibration meter," *J. Meas. Eng.*, vol. 11, pp. 51-61, Dec. 2022.

[5] N. Meier and A. Georgiadis, "Automatic assembling of bearings including clearance measurement," *Procedia CIRP*, vol. 41, pp. 242-246, Feb. 2016.

[6] Y. Ren, P. Zhang, B. Shao, X. Liu, X. Lei, H. Liu, and W. Zou, "Correlation-changed-EMD algorithm for single frequency-sweep interferometry signal of high-speed rotating structure clearance measurement," *IEEE Sens. J.*, vol. 23, pp. 29366-29375, Oct. 2023.

[7] S. Lavagnoli, G. Paniagua, M. Tulkens, and A. Steiner, "High-fidelity rotor gap measurements in a short-duration turbine rig," *Mech. Syst. Signal Pr.*, vol. 27, pp. 590-603, Oct. 2012.

[8] J. Passenbrunner, S. Silber, and W. Amrhein, "Investigation of a digital eddy current sensor," in *Proc. IEEE Int. Electric Mach. Drives Conf. (IEMDC)*, Coeur d'Alene, USA, May 2015, pp. 728-734.

[9] L. Wang, Y. Yan, Y. Hu, and X. Qian, "Intelligent condition monitoring of rotating machinery through electrostatic sensing and signal analysis," in *Proc. IEEE Int. Conf. Smart Instrum., Meas. Appl. (ICSIMA)*, Kuala Lumpur, Malaysia, Nov. 2013, pp. 1–4.

[10] Y. Hu, Y. Yan, L. Wang, X. Qian, and X. Wang, "Simultaneous measurement of belt speed and vibration through electrostatic sensing and data fusion," *IEEE Trans. Instrum. Meas.*, vol. 65, pp. 1130-1138, May 2015.

[11] L. Wang, Y. Yan, Y. Hu, and X. Qian, "Radial vibration measurement of rotary shafts through electrostatic sensing and Hilbert-Huang Transform," in *Proc. IEEE Int. Instrum. Meas. Technol. Conf. (I2MTC)*, Taipei, Chinese Taiwan, May 2016, pp. 1–5.

[12] K. Reda and Y. Yan, "Vibration measurement of an unbalanced metallic shaft using electrostatic sensors," *IEEE Trans. Instrum. Meas.*, vol. 68, no. 5, pp. 1467-1476, May 2019.

[13] L. Wang, M. Hu, K. Kong, J. Tao, K. Ji, and Z. Dai, "A deep-learning-assisted versatile electret sensor for moving object detection," *Nano Energy*, vol. 104, Dec. 2022, Art. no. 107934.

[14] J. Lowell and A. Brown, "Contact electrification of chemically modified surfaces," *J. Electrost.*, vol. 21, pp. 69-79, Feb. 1988.

[15] W. Greason, "Investigation of a test methodology for triboelectrification," *J. Electrost.*, vol. 49, pp. 245-256, Mar. 2000.

[16] L. Zhang, G. Chen, H. Xiao, B. Cai, H. Huang, and L. Wu, "Preparation and charge storage property of FEP thin film electret with grid electric field distribution in millimeter scale," *Acta Phys. Sin.*, vol. 64, Nov. 2015, Art. no. 237701.

[17] C. Dias, J. Marat-Mendes, and J. Giacometti, "Effects of a corona discharge on the charge stability of Teflon FEP negative electrets,". *J. Phys. D: Appl. Phys.*, vol. 22, pp. 663-669, 1989.

[18] X. Liu, Y. Yan, Y. Hu, and L. Wang, "Optimization of Electrostatic Sensors for Rotational Speed Measurement of a Metallic Rotor," *IEEE Trans. Instrum. Meas.*, vol. 73, Dec. 2023, Art. no. 9501811.